

The Anatomy of a Freezing Lead

ANTHONY J. GOW, DEBRA A. MEESE, DONALD K. PEROVICH, AND WALTER B. TUCKER III

U.S. Army Cold Regions Research and Engineering Laboratory, Hanover, New Hampshire

Winter leads are regions of intense ice growth with resultant large fluxes of heat to the atmosphere and salt to the ocean. They constitute a major source of new ice in the Arctic basin. During the 1988 drift phase of the Coordinated Eastern Arctic Experiment we were afforded a unique opportunity to conduct a detailed, long-term study of a freezing lead. Measurements were made from September 17 to November 18, during which time the ice grew from open water to a thickness of 0.56 m. Cores were removed from the lead ice on a routine basis and analyzed for ice temperature, salinity, density, and structure. From these measurements the derived quantities of brine volume, porosity, heat flux to the atmosphere, and salt flux to the ocean were computed. In addition to this 2-month time series study of ice cores, the spatial variation in lead ice properties was investigated on September 30. Thin-section studies of ice structure indicated that the upper 0.05–0.15 m of the ice sheet was granular and that the lower portion was columnar. Typically, a portion of the granular layer was snow ice. Once the transition from granular to columnar ice had occurred, granular ice did not reappear. As the ice grew thicker the *c* axes of the ice crystals became aligned within the horizontal plane. This alignment direction corresponded closely with the inferred direction of the current at the ice/water interface. Vertical temperature profiles in the ice were approximately linear. Salinity profiles were usually C-shaped with bulk salinities ranging from 9 to 6‰, before stabilizing at 6‰ for ice thicker than 0.35 m. Core data were used to compute the flux of heat to the atmosphere and the flux of salt to the ocean for seven time intervals during the experiment. Heat fluxes ranged from 89 to 29 W/m² with an average of 50 W m⁻², roughly 3 times the corresponding value from multiyear ice. The flux of salt from the lead ice to the ocean varied from 0.51 to 0.06 kg m⁻² d⁻¹, averaging 0.21 kg m⁻² d⁻¹.

INTRODUCTION

Leads are an important component of the Arctic pack ice regime. During winter, leads and polynyas constitute the only sources of open water within the Arctic basin, and it is here that the highest rates of ice production occur. *Maykut* [1982] estimates that the total annual ice production associated with open leads and young ice (0–0.8 m) is nearly twice that of thicker ice. Most of this growth occurs during fall and winter when open water and thin ice make up only a small fraction of the total ice budget. *Maykut's* calculations show that turbulent heat losses to the atmosphere during fall and winter total about 200 MJ m⁻², most of which arise from heat conducted from the ocean to the surface, through the thin ice. The ice production and heat loss to the atmosphere are more than an order of magnitude larger for a freezing lead than for thicker (3–4 m) multiyear ice [*Maykut*, 1978]. Likewise, the salt rejected into the ocean resulting from young ice production far exceeds that for thicker ice. In a theoretical study, *Maykut* [1982] determined that to properly model temporal changes in the mixed layer, it was necessary to include young ice.

The regional mechanical behavior of the ice pack as a continuum is largely dependent on leads. The distribution of ice thicknesses and open water determines the rheological behavior of the ice by virtue of its control of the regional strength. The large-scale strength is very low if the concentration of leads and thin ice is relatively high. As the ice converges, it is the young ice which deforms to create ridges. Ridging increases the regional thickness, resulting in an increase in the regional ice strength. However, our understanding of the relationship between lead formation, ice

growth, pressure ridging, and stress transfer within the pack is meager.

There are many unanswered questions regarding ice production processes and the relationship between ice growth and heat and salt fluxes. A large unknown is the role of frazil in Arctic leads. Frazil originates by nucleation of ice crystals in supercooled, turbulent water. When aggregates of frazil crystals consolidate, either partially or completely by freezing, the resultant product is called frazil ice. We know, for instance, that frazil ice production constitutes a large part of the ice mass balance in the Weddell Sea [*Gow et al.*, 1982; *Lange et al.*, 1989]. Frazil has not been found in such prolific amounts in sea ice from the central Arctic. However, new ice growing in leads generally starts as frazil [*Weeks and Ackley*, 1986]. This is significant because in the presence of a wind field, frazil can also be herded to one side of the lead, maintaining an area of open water with attendant large heat losses to the atmosphere. In this fashion, extremely large rates of ice production can be maintained. We do not understand how frazil production may vary under different environmental conditions such as wind, current, and wave action and for different lead geometries. Similar questions can be raised regarding the temporal and spatial variations of other properties of freezing leads. These include ice thickness, crystal structure, physical properties, and chemical composition.

We were afforded a unique opportunity to examine a freezing lead in detail during the drift phase of the Coordinated Eastern Arctic Experiment (CEAREX), which took place in the fall of 1988. To facilitate this drift phase component of the experiment, the Norwegian research vessel *Polarbjorn* was maneuvered alongside and moored to a large fragment of multiyear ice located in fairly compact pack ice several hundred kilometers off the northeast coast of Spitsbergen. The positioning and mooring took place on Julian day 260 (hereafter simply referred to as day 260)

This paper is not subject to U.S. copyright. Published in 1990 by the American Geophysical Union.

Paper number 90JC01271.

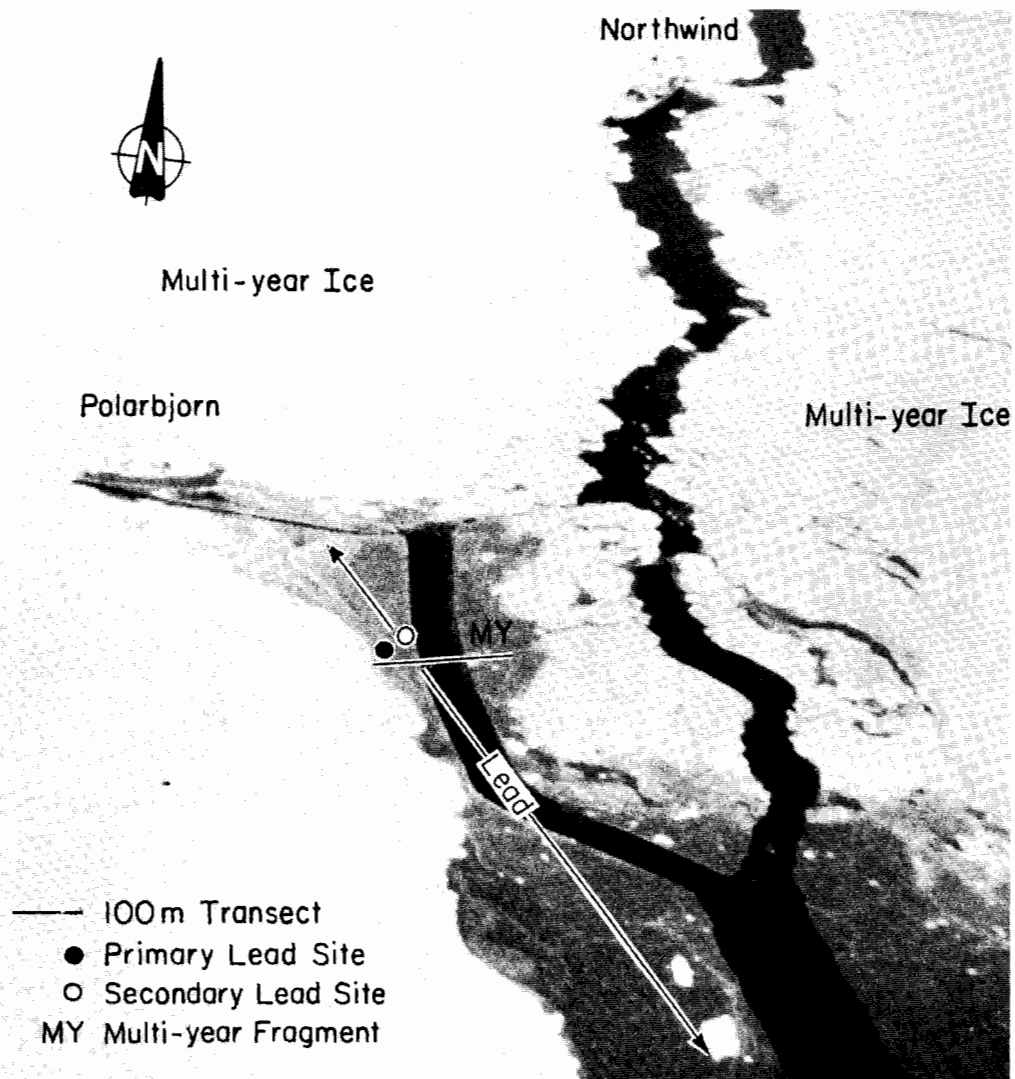


Fig. 1. Aerial photograph, taken on Julian day 262 (September 18, 1988), of the lead and surrounding multiyear ice. At this time the lead ice was less than 0.10 m thick. The channel traversing the lead was originally created by a small power boat used to make oceanographic measurements on September 18. It subsequently diverged to the width, as photographed, before freezing. The photograph is courtesy of D. Bell.

(September 16, 1988), with assistance from the United States Coast Guard Icebreaker *Northwind*. At this time a small unfrozen lead, created by recent fracturing of a large multi-year floe, extended for a distance of several hundreds of meters off the starboard side of *Polarbjorn*. The situation as it existed on day 262 is indicated in the aerial photograph (Figure 1) showing the lead now covered over with a thin layer of sea ice less than 0.10 m thick. The lead ice continued to grow undisturbed until day 265 when ice conditions permitted the first preliminary measurements of ice thickness and related physical and structural properties to be made. Beginning the evening of day 265 some localized deformation resulted in the formation of a rubblelike feature of rafted ice blocks located 60–80 m out from the edge of the lead. Following this rubbing event the lead stabilized, and full-scale investigation of its ice cover, including profile measurements of its temperature, salinity, density, chemistry, and structure, were initiated on day 268. These investigations were maintained, uninterrupted, for the next 2 months until day 323 (November 18), when the area of ice in

the immediate vicinity of *Polarbjorn* underwent very severe deformation that led eventually to breakup of the ice and termination of the experiment. From the time of its insertion in the ice to the onset of breakup, *Polarbjorn* drifted from 82° 40' N, 32° 32' E, to 78° 54' N, 31° 27' E. The timing of the drift afforded us a unique opportunity to observe and make measurements of lead freeze-up during the Arctic fall-to-winter transition period when leads throughout the Arctic basin are undergoing intense ice growth with resultant large fluxes of heat to the atmosphere and salt to the ocean.

EXPERIMENTAL TECHNIQUES

All samples used during the present investigations were obtained by coring through the frozen lead. This drilling included 16 cores taken for comprehensive studies of growth properties over a 2-month period at a single location, the time series site, and a total of 18 ice cores drilled along a 100-m-long traverse for the purpose of examining spatial variations in the thickness, salinity, and crystalline structure

of ice across the lead. Cores measuring 105 mm in diameter were obtained through the entire thickness of the ice using a Cold Regions Research and Engineering Laboratory (CRREL) fiberglass auger. In situ ice temperatures were measured as soon as a core was pulled from the ice sheet by inserting a digital thermometer probe into holes drilled into the side of the core at intervals of 0.05–0.10 m. These vertical temperature profile measurements were made with an estimated accuracy of $\pm 0.1^\circ\text{C}$. Occasionally, when ambient air temperatures rose above -10°C , a second core was taken and sectioned immediately for salinity measurements in order to minimize brine drainage effects. Generally, however, cores were placed in tubes and returned to the ship where a core processing facility had been set up to examine the crystalline structure of the ice and to prepare samples for density and salinity measurements. Once on board ship the freshly drilled cores were logged and examined visually for significant stratigraphic features such as growth banding, evidence of rafting, bubbiness, and sediment and algal layers. The ends of individual core pieces were carefully matched, and the whole core was then oriented and marked before cutting it into 0.10-m-long pieces for density and salinity measurements. A circular cutoff saw was used to ensure the parallel end cuts needed to obtain density measurements to an accuracy of $\pm 0.005 \text{ Mg m}^{-3}$. Densities were determined by first weighing the 0.10-m-long sections on a digital balance with a readout precision of 0.1 g and then measuring the length and diameter of the cylindrical core piece with digital calipers accurate to $\pm 0.02 \text{ mm}$. Vertical sections were then sliced off the side of each individual core piece with a band saw and examined between crossed polarizers on a light table. This technique permits the identification of granular and columnar ices on the basis of their diagnostic crystalline textures, from which observations of the relative proportions of each ice type can be determined. The next step was to cut horizontal samples at locations selected on the basis of the vertical thick-section structure examination and to slice these samples into thin sections (0.2–0.5 mm thick) on a microtome. These sections, used primarily for determining petrographic details of the ice, were then photographed between crossed polarizers for record purposes and later analysis. Full details of thin-sectioning procedures, crystal orientation analysis, and photographic documentation of structure are given by Weeks and Gow [1978] and Gow *et al.* [1987*a, b*].

The remaining pieces of core from which vertical and horizontal sections had been sliced were placed in containers and melted for salinity measurements. Salinities were determined from conductivities measured on a Beckman Solubridge that was periodically calibrated against solutions prepared from Copenhagen standard seawater (chlorinity, 19.375‰). All salinities were corrected to a reference temperature of 25°C . Measurement precision is estimated at $\pm 0.2\text{‰}$.

RESULTS AND DISCUSSION

Observations on Day 315

An illustration of the kinds of profile measurements made in the lead ice is shown in Figure 2 for a core taken on day 315. Structurally, the ice on this date consisted of 0.05 m of granular ice overlain by 0.03 m of snow and underlain by

0.49 m of columnar ice. The granular ice originated by consolidation of frazil crystals formed in the water column as a result of turbulent freezing in wind-roughened seas. Further freezing consolidated the frazil crystals, creating a layer of stabilized frazil ice 50 mm thick, which covered this part of the lead. This was followed almost immediately by congelation growth, that is, freezing of seawater directly to the bottom of the frazil ice sheet. Texturally, congelation growth typically gives rise to columnar-shaped, vertically elongated crystals. It should be noted that once the transition from frazil to congelation ice had taken place, no reappearance of frazil was observed. When the columnar ice reached thicknesses of 0.35–0.40 m, the *c* axes of the crystals started to become aligned. Crystal orientation measurements on cores carefully oriented in azimuth by compass showed a strong north-south alignment of *c* axes. This alignment closely paralleled the direction of the current at the ice/water interface as inferred from both the dominant south-southwest drift of the ice pack (during which time the constancy of the ship's heading indicated that little significant rotation of the ice pack was occurring) and the current measurements made in the oceanic hydroholes (M. G. McPhee, personal communication, 1990).

The temperature profile in the ice was essentially linear with a near-surface temperature of -10°C on day 315. The salinity profile was C-shaped, a characteristic feature of most cores. The bulk salinity was 6.5‰ with brine volumes of individual sections ranging from 2.8 to 7.9%. Density measurements yielded values in the range 0.90–0.92 Mg m^{-3} , equivalent to porosities (entrapped air contents) of less than 3%.

Spatial Variability

Measurements at 18 sites along a 100-m transect were made on day 274 in lead ice that was relatively smooth-surfaced except for an area of rubbly ice located between 60 and 80 m along the transect. This rubbled ice resulted from the interaction of thin lead ice with a small piece of multiyear ice, which from its size and location probably corresponds to the small floe marked MY in Figure 1. The narrow channel near the floe soon refroze, incorporating the small multiyear floe which was subsequently overridden by blocks of thin (0.15–0.20 m thick) lead ice during a period of localized deformation on day 265. The weight of rafted blocks was sufficient to depress the top of the multiyear floe below sea level. The bottom of the floe was not penetrated by drilling, but its thickness is estimated at 1.5–1.7 m on the basis of measurements of thickness of the multiyear ice bordering the lead. Results from spatial variability studies of the structural, thermal, and salinity characteristics of the lead are presented in Figure 3.

Structurally, as demonstrated in Figure 3*a*, the lead everywhere, except for the area of rubbled ice, consisted of variable amounts of granular ice overlying columnar ice. The granular ice thickness increased from 0.21 m at the edge of the lead to a maximum of 0.33 m from the edge before decreasing progressively to a minimum of 0.03 m at 15 m along the transect. By 20 m it had increased to 0.15 m, decreasing again to 0.06 m at 30 m and then never exceeding 0.10 m for the remainder of the transect. These data clearly indicate some variability in the granular ice content. For this particular lead the variability was primarily a result of snow

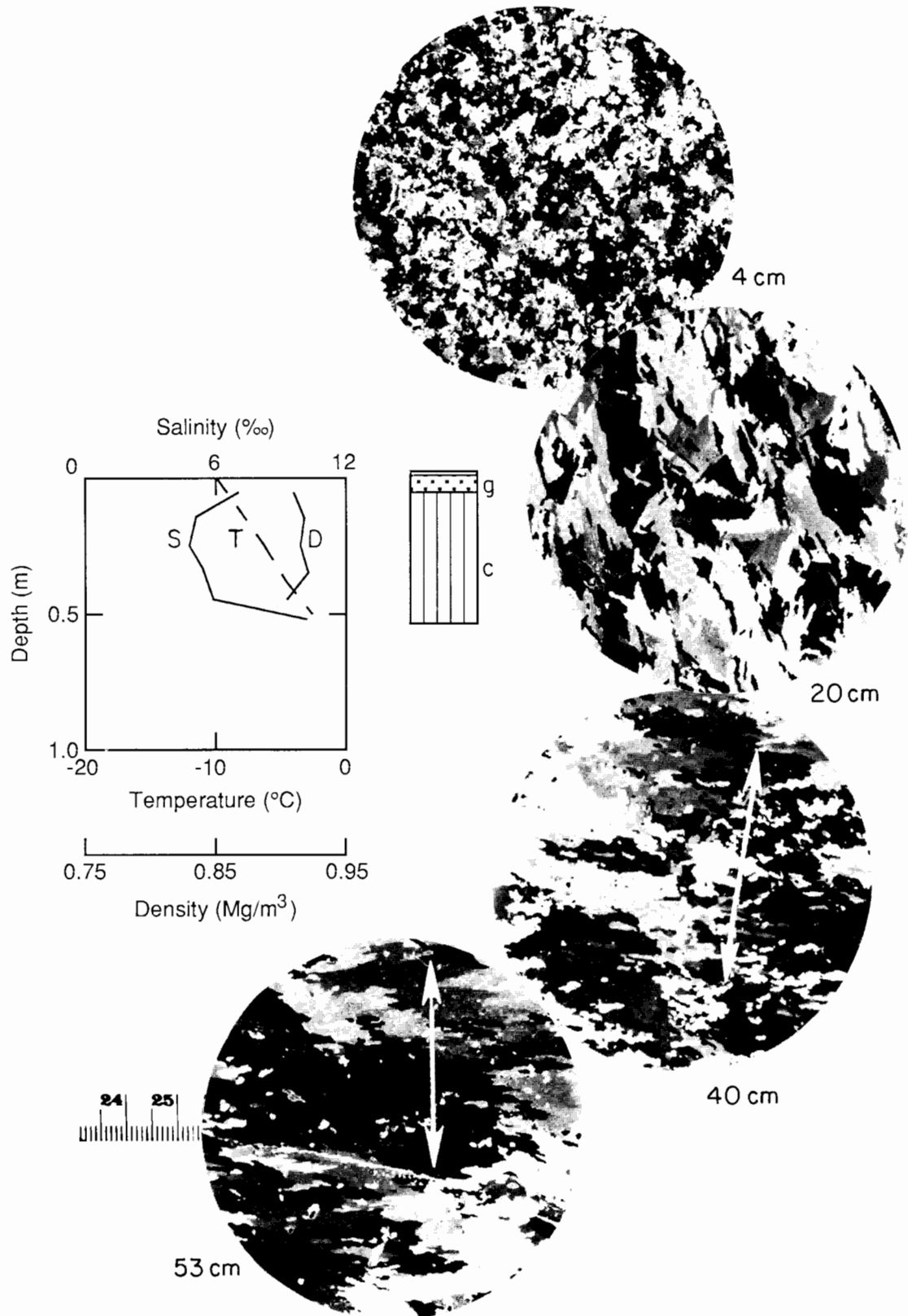


Fig. 2. Physical property and structural profiles of lead ice measured on Julian day 315. The salinity, temperature, and density profiles are designated by the symbols S, T, and D, respectively. Symbols g and c beside the structure profile denote granular and columnar ice, respectively. The four horizontal thin-section photographs were taken at the depths indicated. Scale subdivisions are in millimeters. Arrows in sections at 0.40 and 0.53 m indicate a predominantly north-south direction of crystal *c* axis alignment.

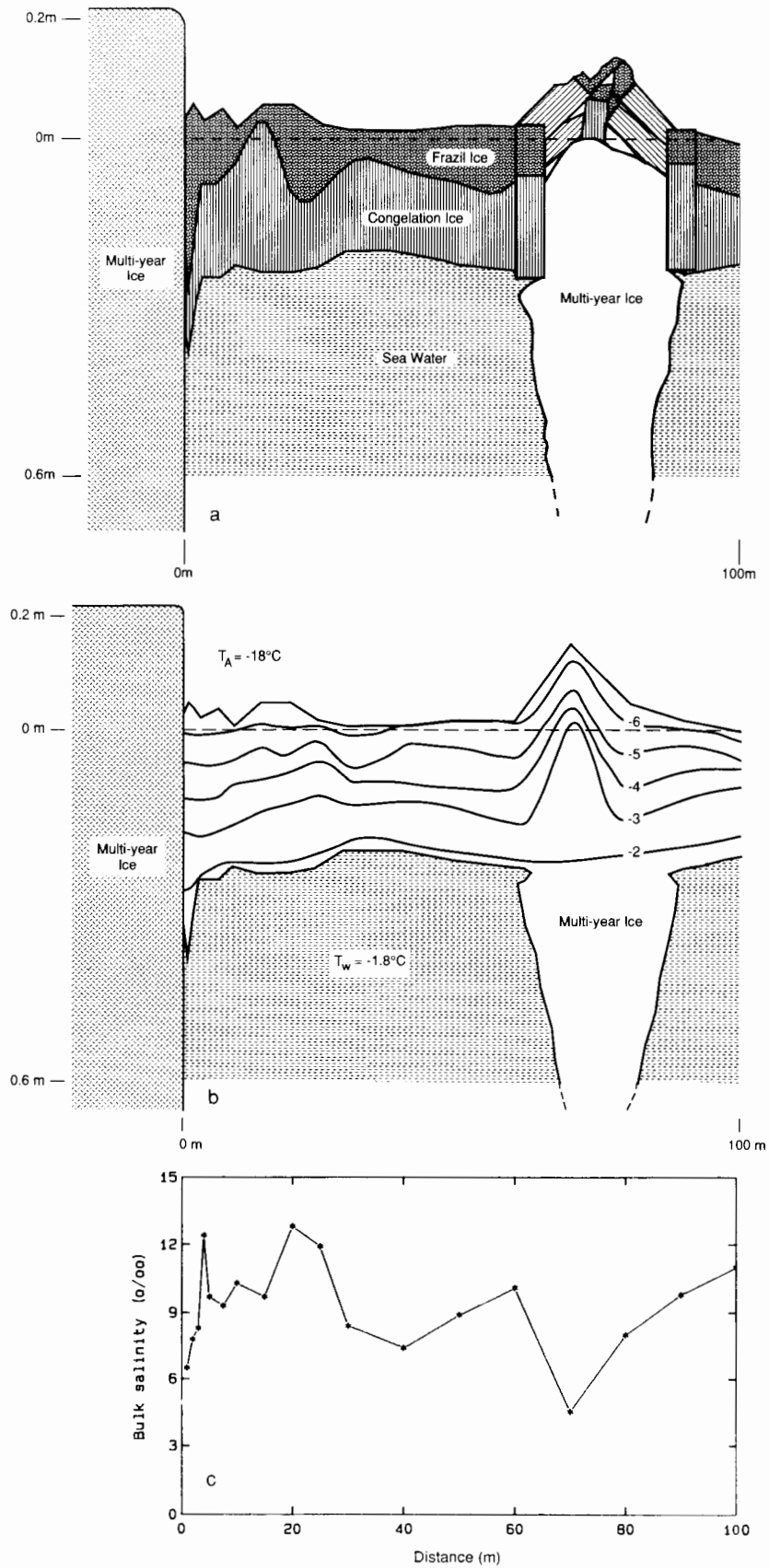


Fig. 3. Results from the 100-m-long transect conducted on day 274. Plotted are the spatial variability of (a) ice composition, (b) temperature, and (c) bulk salinity. There is a 100:1 exaggeration in the vertical scale in Figures 3a and 3b.

blowing off the edge of the multiyear ice bordering the lead. At the edge of the lead adjacent to the multiyear floe the weight of snow was sufficient to depress the top of the ice sheet below its freeboard, allowing seawater to infiltrate the snow and to convert it into saline snow ice. Another mechanism which can contribute to spatial variations in frazil content is the herding of frazil in the lead by wind and wave action. Frazil did not reappear once the transformation to congelation ice had taken place. The congelation ice was characteristically columnar with the *c* axes of crystals at the bottom of the thicker congelation sequences showing a tendency to become oriented within the horizontal plane. However, no alignments of *c* axes, indicative of directional current action at the ice/water interface, were observed at this growth stage (day 274) of the lead ice.

The spatial temperature distribution in the ice along the undeformed section of the 100-m-long transect (Figure 3b) shows minor perturbations related mainly to changes in surface topography and thickness. The notable exception occurs in the zone of rubble ice where the rafting of ice blocks on and around a fragment of multiyear ice has caused a major disruption in the thermal characteristics of this part of the lead. The unbroken nature of cores obtained in this zone on day 274, only 9 days after its formation, testifies to the consolidated condition of the rafted ice blocks in the rubble field. However, the perturbations in the thermal field resulting from this activity, incurred on day 265, were still very much in evidence on day 274.

Bulk salinities, plotted as a function of distance along the 100-m-long transect (Figure 3c), show appreciable variations linked partly at least to spatial variations in the crystalline texture of the ice. Sites exhibiting bulk salinities exceeding 10‰, for example, those located at 4, 10, 20, 25, 60, and 100 m along the transect were all characterized by very high salinities of 15‰ or more in the top 0.10 m, most likely related to the occurrence of brine-soaked snow and/or brine-rich frazil. At all other sites except one, salinities in the top few centimeters exceeded 11‰; congelation ice salinities, on the other hand, rarely exceeded 8‰. By far the lowest bulk salinity (4.5‰) was measured at the 70-m site located near the center of the rubble field where the core included segments of multiyear ice with salinities averaging around 3‰. In rafted ice blocks at this site and at the 80-m site where only the rafted ice block section at the edge of the rubble field was sampled, salinities averaged 9‰. Excluding data from the rubble field, the thickness of ice along the 100-m-long transect averaged 0.26 m on day 274; its salinity averaged 9.6‰.

Time Series Measurements

Results of time series observations of lead ice growth characteristics at a single location over a 2-month period are displayed in Figures 4a–4d. Air temperatures (P. Guest, personal communication, 1988) for this period are plotted in Figure 4a and display an overall decrease in temperatures with monthly mean values of -11.9°C for the latter half of September, -19.6°C for October, and -25.3°C for November. There was one distinct warming event around day 311, when temperatures increased from -30°C to -15°C over a 2-day period.

Temperature data from the ice core measurements were used to determine the temperature field within the ice. Figure 4b displays temperatures in the lead ice as a function of depth and time. Spatially, vertical temperature gradients

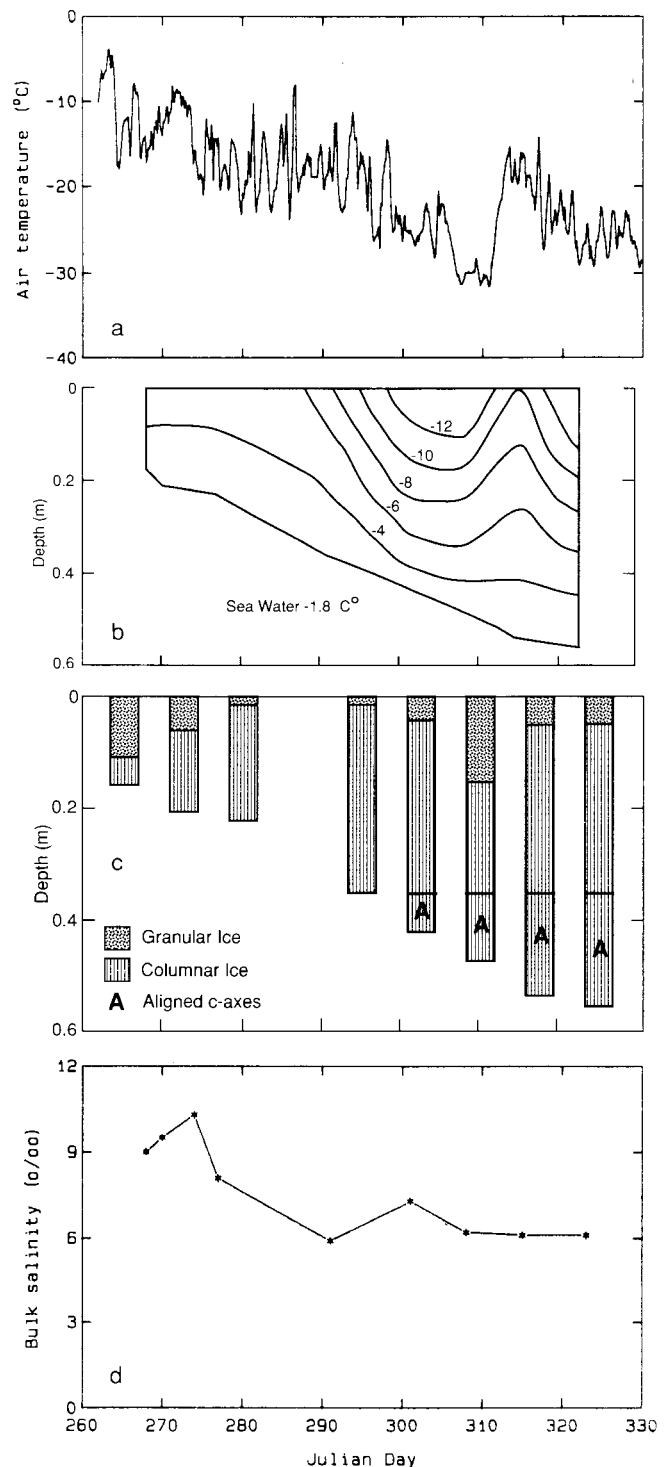


Fig. 4. Summary of time series measurements of lead ice from day 265 to day 323: (a) air temperature, (b) ice temperature and ice thickness, (c) ice composition, and (d) bulk salinity.

were essentially linear, while temporally, there was a general cooling of the ice as air temperatures decreased and the ice grew thicker. The cooling trend in the ice was interrupted by the warming event on day 311, after which temperatures continued to decrease.

Representative structure profile measurements (Figure 4c) show that granular (principally frazil) ice overlays columnar ice in all cores. From these and additional observations it can be seen that the frazil ice component varied appreciably

in thickness (0.02–0.15 m) at this one general location. This variability is due to the fact that cores were not taken from exactly the same location. We centered our sampling on an area of about 5 m² located 6–7 m out from the edge of the lead, and in this case it appears that frazil ice thickness can vary significantly over relatively short distances. As described earlier, this situation was even more apparent in the measurements made along the 100-m traverse.

The ice thickness profile in Figure 4b shows that following a short period of rapid growth initially (0.15 m in about 4 days), the growth rate decreased, averaging 7.5 mm d⁻¹ from day 265 to day 315. Growth during this period was entirely due to the formation of congelation ice which, by day 323, constituted 91% of the ice volume in this part of the lead. The onset of aligned *c* axes occurred during the period between day 291 and day 301. Strongly aligned *c* axes were first observed at 0.40 m depth on day 301, and this alignment persisted through to the last day of measurements (day 323) when the ice thickness measured 0.56 m. As mentioned earlier, the alignment was in the direction of the inferred and measured current at the ice/water interface.

Bulk salinities of lead ice sampled during the 2-month observation period are presented in Figure 4d. The bulk salinity (S_b) of an ice cover is defined as

$$S_b = (1/H) \int S_i(z) dz \quad (1)$$

where S_i is the ice salinity (per mil), H is the ice thickness (meters), and z is the vertical dimension. Since ice salinities were measured incrementally down the entire length of a core, the bulk salinity for the total ice thickness can be calculated from

$$S_b = (1/H) \sum_j S_{ij} \Delta z_j \quad (2)$$

where S_{ij} and Δz_j are the salinity and thickness of a layer j , respectively. The resultant plot shows relatively high salinities initially, peaking at about 11‰ in ice that is 0.21–0.23 m thick (around day 273) and then dropping to 8‰ by day 277 in ice that is 0.24 m thick. By day 291 when the ice was measured to be 0.34–0.36 m thick, the bulk salinity had decreased further to about 6‰, where it essentially remained until the end of experiment (day 323) and by which time the ice had grown to a thickness of 0.56 m.

As mentioned earlier, salinity profiles were characteristically C-shaped because of the appreciably higher salinities measured at the top and bottom of the ice column. High salinities at the top of the ice can probably be attributed in this instance to a combination of factors, including enhanced salinities in the top layers of granular ice (frazil and brine-rich snow ice), elevated levels of brine entrapment accompanying the relatively rapid rates of growth in the top 0.10 m or so of congelation ice, and expulsion of brine onto the surface following freezing. A subsequent decrease in the bulk salinity after about 0.20 m of ice growth coincides closely with the observed establishment of a near-constant rate of freezing in the lead. Stabilization of the bulk salinity at about 6‰ occurred once the ice sheet had thickened to around 0.35 m. However, salinity profiles in thicker ice, for example, the day 315 profile, still display basal ice salinities well in excess of 6‰, indicating either that some process of downward migration of brine must be occurring to maintain

a constant bulk salinity of about 6‰ or that enhanced salinities in the basal ice do not accurately reflect the brine content of freshly frozen sea ice.

Our results are in general accord with both field [Cox and Weeks, 1974] and laboratory [Cox and Weeks, 1975] observations that predict a decrease in bulk salinity as the ice grows thicker. However, more interesting is the establishment of quasi-stable salinities in ice thicker than about 0.35 m. This is in close agreement with observations at Hopedale, Labrador, by Weeks and Lee [1958] for ice between 0.35 and 0.85 m thick, representing the bulk of the winter ice growth. This situation is also strikingly demonstrated in results reported by Nakawo and Sinha [1981] for an entire winter's ice growth at Eclipse Sound, near Pond Inlet, Baffin Island. From repeated measurements made at a large number of specified levels in the growing ice sheet, Nakawo and Sinha [1981] convincingly demonstrated that the salinity essentially stabilized at around 6‰ at about 0.40 m depth. This quasi-stable salinity, which persisted to approximately 1.0 m depth, is consistent with an essentially linear rate of ice growth. The small decrease to values of around 5‰ that they observed below 1.0 m can be readily attributed to decreased rates of ice growth measured between 1.0 and 1.5 m. According to Nakawo and Sinha [1981], significant desalination of the ice sheet did not occur until the onset of warm temperatures later in the spring.

Nakawo and Sinha [1981] also observed very high salinities (up to 24.7‰) in the basal ice of most cores. They considered these high salinities to be an indication of the high brine content of freshly frozen ice. However, closer examination of their salinity profiles shows that elevated salinities measured at the bottom of growing sea ice were invariably confined to the basal 20–30 mm of growth. In congelation ice this constitutes the highly permeable skeletal layer consisting of vertically oriented platelike dendrites between which brine is able to circulate freely. In freshly drilled core there is a tendency for capillary effects to retain this interdendrite brine in amounts which can greatly exceed that which is finally incorporated into the ice following the narrowing of the interdendrite grooves and the sealing off of the brine pockets as freezing progresses. If this retention by capillary action in fact occurs when freshly cored bottom ice is transferred into containers to prevent loss of brine by drainage, then the resultant elevated salinities actually reflect a transient situation only, not the final freeze-in value. Bottom cores that are allowed to "sit around," i.e., that are not transferred immediately to containers to prevent loss of brine, usually yield salinities more similar to those measured in the body of the ice sheet. Some support for the idea that the bulk salinity is actually determined in thicker ice by the volume of brine trapped when the brine pockets become sealed off from the interdendrite grooves derives from our observation that the near-constant bulk salinity of 6‰ we measured in lead ice thicker than 0.35 m agrees closely with bulk salinities measured in 1.5- to 2.0-m-thick sea ice sheets in the Arctic and the Antarctic [Gow and Tucker, 1990]. We hasten to point out that our observation of a constant bulk salinity in lead ice thicker than 0.35 m does not diminish brine drainage under gravity as a viable mechanism in warm ice, only that it exerts much less control maintaining a constant bulk salinity in cold winter ice than C-shaped profiles have led us to believe. In short, quasi-stable salinities observed in thicker winter ice profiles actually reflect a

TABLE 1. Summary of Heat and Salt Flux Calculations for the Lead

Day	H_i , m	dh_i/dt , mm d ⁻¹	Heat				Salt		
			Q_i , MJ m ⁻²	F_i , W m ⁻²	F_w , W m ⁻²	F_c , W m ⁻²	S_b , ‰	S_r , kg m ⁻²	S_f , kg m ⁻² d ⁻¹
261	0.00		0	79	10	89	0.0000	0.00	0.51
268	0.17	24.3	48	19	10	29	0.0090	3.59	0.16
277	0.23	6.7	63	35	20	55	0.0081	5.04	0.26
291	0.36	9.3	105	31	26	57	0.0059	8.62	0.11
301	0.43	7.0	132	26	15	41	0.0073	9.74	0.23
308	0.48	7.1	148	20	16	36	0.0062	11.36	0.21
315	0.54	8.6	160	16	24	40	0.0061	12.83	0.06
323	0.56	2.5	171				0.0061	13.30	

Day is the Julian date, H_i is the ice thickness, dh_i/dt is the growth rate, Q_i is the total amount of heat per unit area liberated by freezing the ice and bringing it to its observed temperature profile, F_i is the corresponding flux, F_w is the oceanic heat flux, F_c is the flux of heat to the atmosphere, S_b is the bulk salinity, S_r is the total salt rejected per unit area, and S_f is the salt flux to the ocean. Values of oceanic heat flux (F_w) were obtained from *Wettlaufer et al.* [1989].

freeze in salinity of about 6‰, which obviates the need for a brine drainage mechanism to offset elevated salinities often observed in the basal 20–30 mm of ice of cold winter sea ice sheets. If brine drainage is an active process at this stage of the ice growth, then it must be limited substantially to the highly permeable basal skeletal layer with little or no significant loss of brine from the overlying ice.

Heat and Salt Fluxes

Freezing leads are areas of intense energy exchange between the ocean and the atmosphere. Under winter conditions, heat losses to the atmosphere through thin ice can be more than an order of magnitude greater than those through multiyear ice [Maykut, 1978]. Likewise, thin ice is a significant factor in determining the net salt flux into the mixed layer.

The surface energy balance of a freezing lead is [Maykut, 1982]

$$F_{ra} + F_L - \xi\sigma T^4 + F_s + F_e = -F_c \quad (3)$$

The conductive heat flux (F_c) is equal to the sum of the fluxes of shortwave radiation that contributes to surface melting (F_{ra}), incoming long-wave radiation (F_L), outgoing long-wave radiation ($\xi\sigma T^4$, ξ is the emissivity, σ is the Boltzmann constant), sensible heat (F_s), and evaporative heat (F_e). For young ice, from late September through May, the turbulent fluxes are the dominant terms in (3) [Maykut, 1978]. Measuring the atmospheric fluxes, however, is a formidable task under any circumstances and is particularly so for thin young ice. While temperature profiles in young ice are usually nearly linear [Maykut, 1978], determining the conductive flux directly ($F_c \propto \partial T/\partial z$) can still be troublesome since it requires a detailed time series of $\partial T/\partial z$. Our data set, from which we can compute $\partial T/\partial z$ only at several discrete times, is not well suited for such a direct determination of F_c .

Fortunately, the ice provides an indirect method of estimating losses to the atmosphere, which requires only measurements of ice thickness, temperature, and salinity. The surface conductive flux is balanced by three terms: (1) the

heat gains or losses in the interior of the ice due to changes in heat content of the ice (F_i), (2) the oceanic heat flux (F_w), and (3) the absorption of shortwave energy in the ice (F_{ri}). More formally, this is expressed as

$$F_c = F_i + F_w + F_{ri} \quad (4)$$

We can calculate the terms on the right-hand side. F_i is the flux of heat due to freezing and cooling of the ice:

$$F_i = dQ_i/dt \quad (5)$$

where Q_i is the total amount of heat (per unit area integrated over depth) liberated by freezing the ice cover and by bringing it to its observed temperature profile:

$$Q_i = \rho \int q_i dz \quad (6)$$

The heat released by freezing a parcel of water and cooling it to temperature T_0 (q_i) is given by *Schwerdtfeger* [1963] as

$$q_i = (L - c_i T_0)[1 - S_i/(\alpha T_0)] + (1/\alpha)S_i(c_w - c_i) \ln [S_i/(\alpha T_0)] \quad (7)$$

where z is depth, ρ is the density of the ice (917 kg m⁻³), L is the latent heat of fusion for pure ice (333.9 kJ kg⁻¹), α is a constant (-0.0182 °C⁻¹), and the specific heat of pure water (c_w) and pure ice (c_i) are 4.23 and 2.01 kJ (kg⁻¹ °C⁻¹), respectively. This expression for q_i was used in (6) and the integral evaluated using the trapezoid rule with a 0.01-m spacing in z . Profiles of $S_i(z)$ and $T_0(z)$ were obtained from the ice core measurements by assuming that the ice salinity was constant within a sampled layer and that the temperature profile was linear between measured values. We computed Q_i at eight times between day 261 and day 323 (Table 1) for which core data were available. F_i was then calculated for each of the seven time intervals using $F_i = \Delta Q_i/\Delta t$.

Values of F_w were obtained from concurrent measurements of oceanic heat flux made by *Wettlaufer et al.* [1989].

They measured mass changes at the underside of the ice and temperature profiles in the ice and water at 12 sites, from which they computed F_w using the methodology of *McPhee and Untersteiner* [1982]. They combined and smoothed their data to generate a time series of the oceanic heat flux. We used their reported $F_w(t)$ to calculate average values for our time intervals (Table 1).

The final term in (4), F_{ri} , represents the absorption of shortwave radiation. Since sea ice is a translucent medium, shortwave radiation penetrates into the interior of the ice and is absorbed, resulting in warming. In general, it is possible to estimate $F_{ri}(t)$ for lead ice by combining observed values of the incident shortwave irradiance with laboratory measurements of light absorption in young ice [*Perovich and Grenfell*, 1981] and theoretical algorithms which predict absorption as a function of ice type and thickness [*Grenfell*, 1979]. However, we believe such detailed calculations are unnecessary for this experiment. Instead, we assume that $F_{ri}(t) = 0$. This assumption is certainly valid for days 293–323 when the Sun had set and there was continual darkness. For the period prior to this we believe that F_{ri} was negligible because of the presence of a snow cover. Spot measurements indicated snow thicknesses in excess of 0.05 m as early as day 265, and results from a snow thickness grid show mean snow thicknesses of 0.08–0.10 m after day 285. Less than 2% of the incident shortwave radiation penetrates a 0.05-m snow cover. Finally, in the earliest stages of ice growth when there was no snow cover, the ice was so thin that the absorbed shortwave energy was a component of the surface energy balance (F_{ra}).

Values of Q_i , F_i , F_w , and F_c for each time period are summarized in Table 1. At first, F_i dominated F_c , but near the end of the experiment the magnitudes of F_i and F_w were comparable. The time series of heat losses to the atmosphere (F_c) is displayed in Figure 5b. The greatest heat losses of 90 $W m^{-2}$ occurred initially, when the ice is the thinnest, after which there was a gradual decrease to values near 40 $W m^{-2}$. If the air temperature and F_w were constant, F_c would decrease as the ice grows thicker. Indeed, this is the general trend of the data. The deviations from this trend result from variations in T_a or F_w . For example, the minimum near day 272 was associated with a few days of warm ($-9^\circ C$) air temperatures. Averaging over the entire 2 months of the experiment gives a mean flux of heat (F_c) to the atmosphere of 50 $W m^{-2}$. For corroboration we also computed F_c directly from the temperature gradient in the ice from $F_c = k \partial T / \partial z$ (using a fresh ice $k = 2.03 W \text{ } ^\circ C \text{ } m^{-1}$) and found that while there were significant differences in the time series of F_c between the direct and the indirect methods, the mean value for the entire period was the same.

Salt rejected by the ice as freezing occurs contributes directly to the oceanic mixed layer. The total amount of salt rejected per square meter (S_r) from an ice cover is

$$S_r = \rho H(S_w - S_b)/1000 \quad (8)$$

where S_w is water salinity (per mil) and 1000 is a scaling factor to convert from per mil to kilograms per kilogram. Applying (8) to our data indicates that a total of 13.3 $kg m^{-2}$ of salt was rejected from the lead ice into the mixed layer between day 261 and day 323. The salt flux S_f is the time derivative of the total salt rejected:

$$S_f = dS_r/dt \quad (9)$$

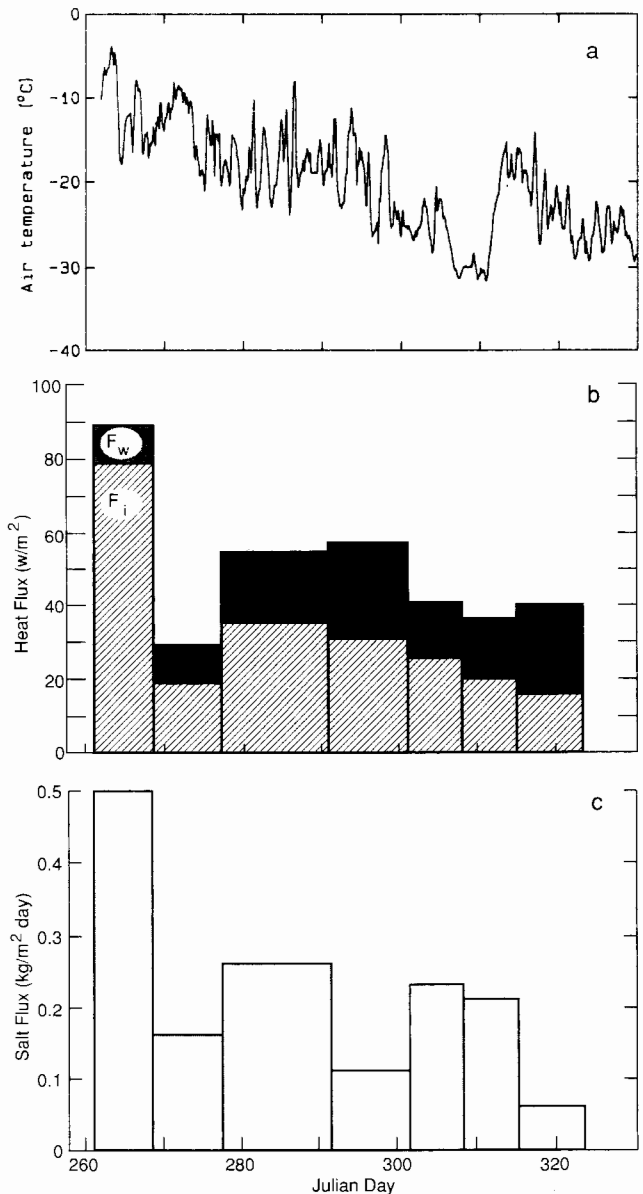


Fig. 5. A time series of heat and salt fluxes for the lead: (a) air temperature, (b) heat flux associated with freezing the ice and bringing it to its observed temperature profile (F_i), oceanic heat flux (F_w), and heat flux to the atmosphere ($F_c = F_i + F_w$), and (c) salt flux (kilograms per square meter per day).

The salt flux as a function of time is plotted in Figure 5c and is summarized in Table 1. Fluxes ranged from 0.51 to 0.06 $kg m^{-2} d^{-1}$ with the largest flux occurring during the initial growth phase when the ice is the thinnest and growth rates are highest. As the ice grows thicker and the growth rate decreases, there is an overall trend toward smaller salt fluxes. Fluctuations from this trend are caused by small-scale spatial variations in salinity and temporal variations in growth rate.

This indirect method of determining heat losses to the atmosphere and salt fluxes to the ocean can be thought of as an integrating technique with the ice recording the integral of the heat and salt fluxes. Though not suited for measurements of high temporal resolution, the method is an effective means of estimating heat losses to the atmosphere and salt fluxes to the ocean averaged over periods of several days. The largest source of error in calculating F_i lies in determining the ice

thickness. We estimate an uncertainty of 5 mm for our measurement, which corresponds, for a typical time interval, to an uncertainty in F_i of approximately 4 W m^{-2} and of $0.02 \text{ kg m}^{-2} \text{ d}^{-1}$ in S_f . Wettlaufer *et al.* [1989] also state that thickness was their largest potential source of error and report uncertainties in F_w of 6 W m^{-2} .

Maykut [1982] theoretically investigated heat and salt fluxes for snow-free young ice. Using thermal forcing representative of the interior of the Arctic Basin, he calculated heat and salt fluxes for ice of different thicknesses. His calculations and our observations are in concert for the initial growth phase from 0.00 to 0.17 m when the observed and predicted heat fluxes were 89 and 77 W m^{-2} and the observed and predicted salt fluxes were 0.51 and $0.44 \text{ kg m}^{-2} \text{ d}^{-1}$, respectively. After this point the observed and predicted fluxes diverged, with predicted values typically being 2–3 times larger. It might be expected that this results from differences in air temperature. However, the mean monthly averages observed during CEAREX were within 2°C of the climatological values used by Maykut. We believe that these differences in fluxes were primarily due to the presence of a 0.05- to 0.15-m snow cover during CEAREX effectively acting as an insulating blanket, giving smaller heat and salt fluxes than those predicted for a snow-free ice cover. In fact, Maykut [1978] estimates that such a snow cover will reduce losses to the atmosphere by approximately 50%, giving good agreement with our observations.

It is illuminating to contrast heat and salt exchange from the lead ice and from the surrounding thick, multiyear ice. For comparison we selected a multiyear site and calculated average values of F_c and S_f for the entire experimental period using the method presented in the heat and mass balance section. While at the primary lead site the ice was growing 0.56 m between day 261 and day 323, there was 0.17 m of bottom ablation on the multiyear ice as it thinned from 1.62 to 1.45 m. This mass loss is a direct consequence of reduced conduction at the bottom of the multiyear ice due to summer heat storage and of the rather large values of oceanic heat flux in this region. The heat loss to the atmosphere from the multiyear ice was only 16 W m^{-2} , approximately one third the mean lead ice value. Because of the bottom ablation and the attendant input of fresh water into the ocean, the salt flux was not only smaller in magnitude but also opposite in sign, with a value of $-0.08 \text{ kg m}^{-2} \text{ d}^{-1}$.

Secondary Lead Site

During the latter part of the experiment a small portion of the lead reopened and then refroze, affording us the additional opportunity of examining and comparing two separate and disparate episodes of freezing within the same lead. Initial ice growth in the primary lead occurred under quiescent conditions, while there was vigorous wind and wave mixing associated with growth in the secondary lead which formed on day 288 when the local winds exceeded 20 m s^{-1} . Structure profiles from day 315 (Figure 6) show a thin layer of columnar, congelation ice at 50–80 mm sandwiched between layers of granular ice. These transitions are clearly documented in the vertical thin-section photograph from 0 to 0.10 m in Figure 6. The initial transition to columnar ice at around 50 mm is consistent with rapid freezing under relatively calm conditions in this part of the lead. We believe the abrupt transition back to granular ice at about 80 mm coincided with the arrival of frazil generated in ice-free areas

of the lead which was subsequently advected to the underside of the existing ice sheet. This resulted in much greater thicknesses of frazil ice than were observed in the primary lead (Figure 2). By day 301, 0.52 m of ice had formed, and on the basis of our examination of thin sections, frazil was still accumulating as of this date. By day 315 the ice thickness had increased to 0.73 m, mainly as the result of growth of columnar ice. A thin section from 0.70 m depth showed the c axes of the crystals to be moderately to strongly aligned. The transition from granular frazil to columnar congelation ice is clearly documented in the vertical thin section from 0.46 to 0.55 m (Figure 6). Despite the fact that this small secondary lead did not form until 27–28 days after the primary lead had frozen over, by day 301, less than 13 days after it opened, ice in the secondary lead was approximately 0.10 m thicker than at the primary lead site; by day 315 it was 0.17 m thicker. These differences simply reflect the rapidity with which frazil can accumulate in a wind-swept lead compared to the purely thermodynamically controlled rates of growth of congelation ice in a quietly freezing lead. This situation has been well documented for the Weddell Sea region of Antarctica, a major source of Antarctic pack ice, where frazil is a major, if not the principal, ice type [Gow *et al.*, 1987b; Lange *et al.*, 1989]. In the Arctic, however, conditions favorable to the widespread production of frazil appear to occur on a more limited scale and mainly in marginal ice zones, for example, the Fram Strait and the Barents Sea [Perovich *et al.*, 1988].

Vertical temperature profiles were essentially linear with temperatures very similar to those observed in older, albeit thinner ice at the primary sampling site. Salinity profiles were remarkably similar to those measured at the primary lead site. This occurs despite the fact that the growth textures of the ice in the two leads are grossly different: substantially granular frazil at the secondary lead site and predominantly columnar congelation ice at the primary lead site. In congelation ice, brine is systematically incorporated between the dendrites of the growing ice crystals, whereas in frazil, seawater becomes trapped in the interstices between the ice grains, leading to a more random distribution of brine inclusions. In this instance it would appear that the salinity of young sea ice was not strongly influenced by differences in the crystalline texture of the ice. Essentially the same situation was reported by Gow *et al.* [1987b] for Weddell Sea pack ice where it was found that frazil ice was not systematically more saline than congelation ice in floes containing both ice types. On day 315 the bulk salinity was 5.6‰ with brine volumes ranging from 2.2% to 5.0%. Densities were more variable than at the primary lead site, ranging from 0.87 to 0.92 Mg m^{-3} . The lower densities are consistent with observations of the widespread occurrence of bubbles and of cavities several millimeters in diameter in the granular frazil, leading to porosities as high as 5.5%. In general, porosities exceeded brine volumes, which is a complete reversal of the situation observed in congelation ice at the primary lead site. This is attributed to basic differences in the ice growth process. In frazil ice where consolidation begins with the adhering and clumping together of individual crystals to form flocs, voids are more likely to occur than in congelation ice formed by direct freezing of water to the underside of the ice sheet.

CONCLUSIONS

The growth characteristics of ice forming in an Arctic lead were studied over the 2-month life span of the lead. Param-

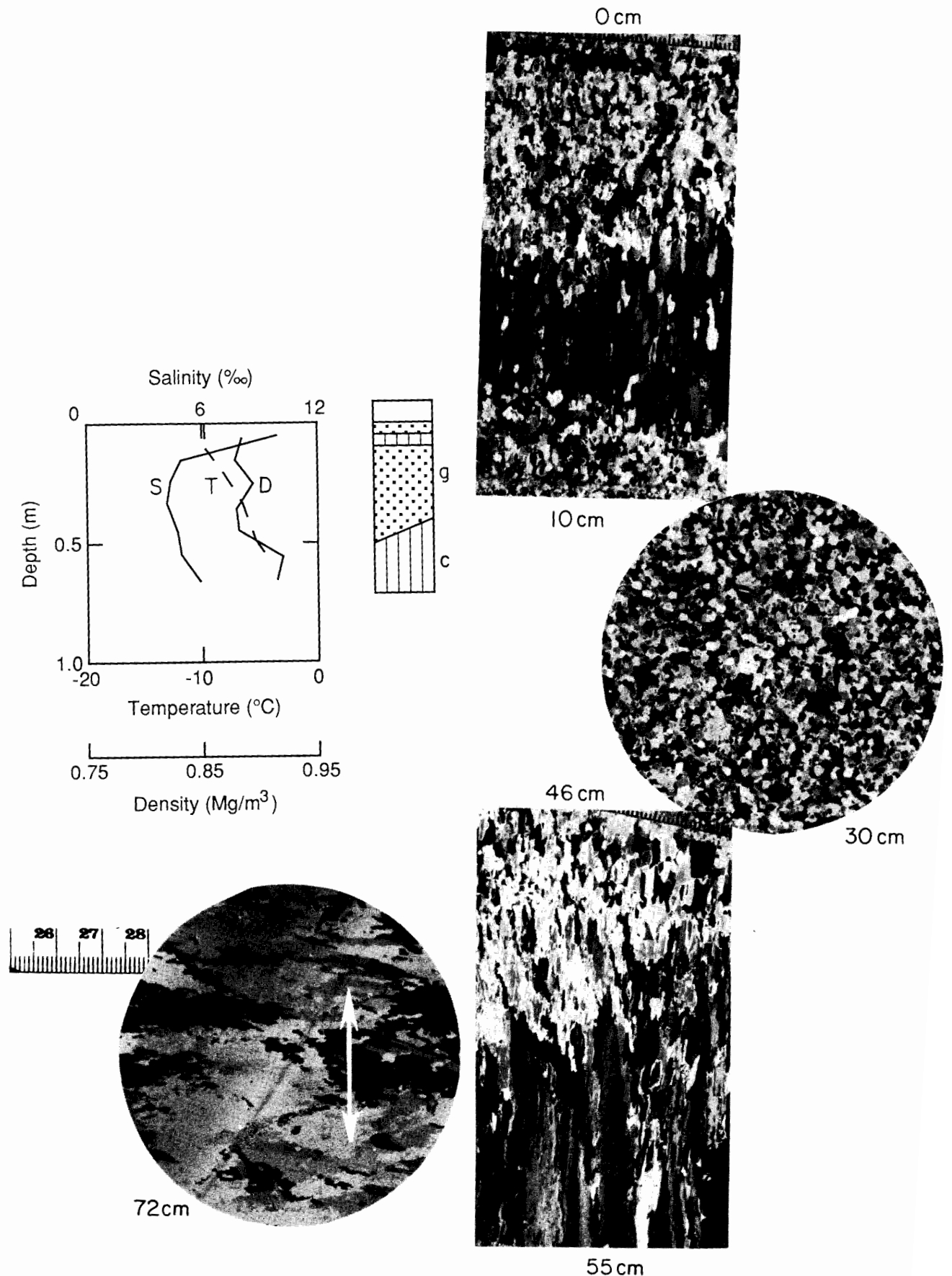


Fig. 6. Physical property and structural profiles of ice at the secondary lead site. Symbols and scale are the same as in Figure 2.

eters measured at the primary sampling site included thickness changes as a function of time, ice structure, temperature, salinity and density profiles, and the derived properties, the fluxes of heat and salt. Spatial variations of properties across the lead were also measured. The maximum thickness measured after 2 months growth was 0.56 m. Structurally, the ice cover consisted of a thin layer of granular ice, mainly frazil averaging 0.05–0.06 m thick, underlain by a substantially thicker layer of columnar congelation ice. At thicknesses greater than about 0.35 m the columnar ice was characterized by aligned *c* axes with the alignment direction closely paralleling the inferred direction of current motion at the ice/water interface. Vertical temperature profiles remained effectively linear over the entire duration of ice growth. Salinity profiles were typically C-shaped with bulk salinities ranging from 9‰ in thinner ice to 6‰ for ice exceeding 0.35 m in thickness. The formation of quasi-stable salinities in the thicker ice is attributed to a near-constant rate of salt entrainment associated with the progressive sealing off of brine pockets in the interdendrite grooves of freshly frozen ice directly above the dendritic growth interface. Densities in congelation ice generally exceeded 0.91 Mg m^{-3} , indicating minimal entrapment of air relative to the volume of entrapped brine. Calculated heat fluxes ranged from 89 to 29 W m^{-2} , and salt fluxes varied from 0.51 to $0.06 \text{ kg m}^{-2} \text{ d}^{-1}$ over the 2-month period. Measurements made along a 100-m-long transect across the lead revealed significant spatial variations in most properties, especially those near the edge of the lead where snow blown off the multiyear ice bordering the lead resulted in enhanced thicknesses of granular ice. Refreezing in a small lead that formed in the main lead about 1 month after the latter had begun freezing over was characterized by frazil ice that accumulated to thicknesses of up to 0.55 m before the onset of congelation ice growth. Once congelation ice growth had commenced, a fairly rapid transition to aligned *c* axis structure was observed.

Certainly, some of our results for this freezing lead are peculiar to the location of the study in the eastern Arctic. For instance, much of the short-term variations in heat flux can be attributed to fluctuations in the air temperature and in the oceanic heat flux. Similarly, variations in the salt flux are due to the changing growth rate as well as to spatial inhomogeneities. We observed that there can be short-term changes in both heat and salt fluxes of up to 50% even when the ice reaches thicknesses of 40 cm. These large variations may be confined to freezing leads in the eastern Arctic or other marginal seas, where atmospheric and oceanic fronts are more common than in the central Arctic. For a midwinter freezing lead in the central pack we would expect more constant air and ocean temperatures, resulting in decreasing heat and salt fluxes as the ice grows thicker.

We believe that other features, such as the spatial variations in properties and processes, are probably typical of most freezing leads. In fact, the focus of this study was a quiescent lead with calm conditions during the initial ice growth and little dynamic activity where spatial variations were relatively minimal. As results from the secondary lead study indicate, conditions in a lead freezing under more active conditions are quite different. The presence of wind during the initial growth phase causes herding of frazil in the lead, resulting in enhanced ice production and large spatial variations in ice thickness across the lead. Dynamic activity

could also result in pressure ridge formation in the young ice or the formation of new leads. These spatial variations would likely produce appreciable spatial differences in heat and salt fluxes within the lead.

Acknowledgments. This work was made possible by support from the Office of Naval Research, Arctic Program, under contract N0001489WM24004. Special thanks go to D. Bell and H. Bosworth for their expert assistance in the field portion of this study.

REFERENCES

- Cox, G. F. N., and W. F. Weeks, Salinity variations in sea ice, *J. Glaciol.*, 13, 109–120, 1974.
- Cox, G. F. N., and W. F. Weeks, Brine drainage and initial salt entrapment in sodium chloride ice, *Res. Rep. 354*, U.S. Army Cold Reg. Res. and Eng. Lab., Hanover, N. H., 1975.
- Gow, A. J., and W. B. Tucker, Sea ice in the polar regions, in *Polar Oceanography, Part A, Physical Science*, edited by W. O. Smith, pp. 47–122, Academic, San Diego, Calif., 1990.
- Gow, A. J., S. F. Ackley, W. F. Weeks, and J. W. Govoni, Physical and structural characteristics of Antarctic sea ice, *Ann. Glaciol.*, 3, 113–117, 1982.
- Gow, A. J., W. B. Tucker, and W. F. Weeks, Physical properties of sea ice in the Fram Strait, June–July 1984, *Rep. 87-16*, U.S. Army Cold Reg. Res. and Eng. Lab., Hanover, N. H., 1987a.
- Gow, A. J., S. F. Ackley, K. R. Buck, and K. M. Golden, Physical and structural characteristics of Weddell Sea pack ice, *Rep. 87-14*, U.S. Army Cold Reg. Res. and Eng. Lab., Hanover, N. H., 1987b.
- Grenfell, T. C., The effects of ice thickness on the exchange of solar radiation over the polar oceans, *J. Glaciol.*, 22, 305–320, 1979.
- Lange, M. A., S. F. Ackley, P. Wadhams, G. S. Dieckmann, and H. Eicken, Development of sea ice in the Weddell Sea, Antarctica, *Ann. Glaciol.*, 12, 92–96, 1989.
- Maykut, G. A., Energy exchange over young sea ice in the central Arctic, *J. Geophys. Res.*, 83, 3646–3658, 1978.
- Maykut, G. A., Large-scale heat exchange and ice production in the central Arctic, *J. Geophys. Res.*, 87, 7971–7984, 1982.
- McPhee, M. G., and N. Untersteiner, Using sea ice to measure vertical heat flux in the ocean, *J. Geophys. Res.*, 87, 2071–2074, 1982.
- Nakawo, M., and N. K. Sinha, Growth rate and salinity profile of first-year sea ice in the high Arctic, *J. Glaciol.*, 27, 315–330, 1981.
- Perovich, D. K., and T. C. Grenfell, Laboratory studies of the optical properties of young sea ice, *J. Glaciol.*, 27, 331–346, 1981.
- Perovich, D. K., A. J. Gow, and W. B. Tucker III, Physical properties of snow and ice in the winter marginal ice zone of Fram Strait, paper presented at IEEE Geoscience and Remote Sensing Society '88 Symposium, Edinburgh, Scotland, Sept. 13–16, 1988.
- Schwerdtfeger, P., The thermal properties of sea ice, *J. Glaciol.*, 4, 789–807, 1963.
- Weeks, W. F., and S. F. Ackley, The growth, structure, and properties of sea ice, in *The Geophysics of Sea Ice*, edited by N. Untersteiner, pp. 1–164, Plenum, New York, 1986.
- Weeks, W. F., and A. J. Gow, Preferred crystal orientations in the fast ice along the margins of the Arctic Ocean, *J. Geophys. Res.*, 83, 5105–5121, 1978.
- Weeks, W. F., and O. S. Lee, Observations on the physical properties of sea ice at Hopedale, Labrador, *Arctic*, 11, 134–155, 1958.
- Wettlaufer, J. S., N. Untersteiner, and R. Colony, Estimating oceanic heat flux from sea ice thickness and temperature data, paper presented at Oceans '89, IEEE International Conference for Understanding the Global Ocean, Seattle, Wash., Sept. 18–21, 1989.

A. J. Gow, D. A. Meese, D. K. Perovich, and W. B. Tucker III, U.S. Army Cold Regions Research and Engineering Laboratory, 72 Lyme Road, Hanover, NH 03755.

(Received January 26, 1990;
revised May 31, 1990;
accepted May 31, 1990.)